The VOL-CALPUFF Model for Atmospheric Ash Dispersal: II. Application to the Weak Mt. Etna Plume of July 2001

S. Barsotti and A. Neri

Istituto Nazionale di Geofisica e Vulcanologia - Sezione di Pisa, Pisa, Italy

S. Barsotti and A. Neri INGV - Sezione di Pisa - Via Della Faggiola 32, 56126 Pisa, Italy

D R A F T   November 20, 2007, 10:01am   D R A F T

Abstract.   The application of the VOL-CALPUFF model (*Barsotti et al.* [2007], this issue) to a weak plume erupted from Mt. Etna in July 2001 is here presented and discussed. The reconstruction of the explosive event was obtained by using high-resolution weather forecasts, produced by a mesoscale non-hydrostatic model, and volcanic source data coming from observations and analytical studies. The plume rise and atmospheric dispersal models were investigated over five days of eruption mostly in terms of column height, aerial ash concentration and ground deposition. Modeling results are shown as a function of various source conditions and compared to independent observations derived from satellite images and deposit mapping. The application of VOL-CALPUFF clearly highlights the crucial role played by meteorological conditions in determining dispersal dynamics. Some of the most important effects described by the model are: a) the large wind field influence on the plume height determination and tilting, b) the contrasting dispersal patterns of ash particles of different sizes, c) the complex and somehow non-intuitive distribution of ash on the ground resulting in preferential directions of dispersal and quite irregular deposit patterns, d) the impossibility to reproduce both the column height and the deposit accumulation pattern by adopting a steady-state vent mass flow rate over the investigated four-day period due to observed temporal changes in eruption dynamics. Modeling results also suggest the need for further integration of simulation outcomes with remote sensing and field reconstructions on ash dispersal processes in future.

1. Introduction

We present the first application of the VOL-CALPUFF model, fully described in the companion paper (*Barsotti et al.* [2007], this issue), to a real event in order to highlight its potentialities and weaknesses. The code originates from the U.S. non-commercial model CALPUFF (*Scire et al.* [2000]), developed and used for air quality applications, modified and developed to make it appropriate for volcanological applications. VOL-CALPUFF is an hybrid code in which a part of the process, i.e. the plume rise phase, is described in a Eulerian framework, whereas dispersal and fallout processes are solved with a Lagrangian approach. Both processes are modelled taking into account the influence of time-dependent, 3D meteorological conditions throughout the duration of the eruption. VOL-CALPUFF relates the computation of the column height, computed by solving the plume theory equations, to the altitude of release of pyroclastic material. The Lagrangian description of the dispersal process guarantees model reliability both close to vent and far from it (*Nguyen et al.* [1997]). The original CALPUFF code was validated through extensive comparison with other widely used codes for air-pollution modeling and through experimental tests concerning passive and active tracer transport and estimation of ground deposition and atmospheric concentrations (*EPA U.S.* [1998]; *Scire et al.* [2000]). Due to its good performance it is currently proposed by the U. S. EPA as a guideline model for environmental applications such as impact studies of proposed and existing pollutant sources. Similarly, VOL-CALPUFF needs to be validated and tested against volcanological applications, and this is a challenge due to the uncertainties when characterizing the natural phenomena.

The paper presents quantitative comparisons between model results and experimental data and observations from the 2001 Etna eruption. This event was characterized by moderately intense explosive activity that produced a weak plume lasting for several weeks. Several recent studies (*Taddeucci et al.* [2002]; *Metrich et al.* [2004]; *Taddeucci et al.* [2004]; *Scollo et al.* [2007]) provide new data and measurements for this event, allowing thorough comparison with VOL-CALPUFF modeling.

In the following section we will illustrate how application of VOL-CALPUFF to this event provides new fundamental insights into the dynamics of the dispersal processes as well as suggests future research needs for data collection and data intercomparison.

2. Mount Etna's 2001 Eruption

The explosive event we refer to started at 1900 LST on 19 July when two pit craters opened on Piano del Lago, on the S flank of Mt.Etna, at about 2570 m asl (see Fig. 1) (*Calvari and Pinkerton* [2004]; *Scollo et al.* [2007]). The first few days of explosive activity, which lasted until 6 August, were characterized by a black and dense ash and lapilli column, of likely phreatomagmatic origin, rising up to 3 km above the vent (*Coltelli et al.* [2001]; GVP/USGS Weekly Volcanic Activity Report - GVP/USGS web-site [2004]; *Scollo et al.* [2007]). During the first days the wind was blowing towards E-NE and the city of Reggio Calabria in the Calabria Region was affected by ash fallout. Due to a wind change on 21 July, the ash cloud started to move S-SE, blanketing Catania on 22 July and creating major problems for the "Fontanarossa" International Airport. The finer portion of ash reached the Island of Malta and then the N Africa coast. The ash cloud evolution was visible on several satellite images and also inferred through deposit characterization studies, making this event suitable for modeling applications. VOL-

70   CALPUFF was applied to simulate the first five days (20-24 July) of this eruption (the

71   tephra fallout on 19-20 July was negligible, see *Scollo et al.* [2007]) in order to describe

72   the main features of atmospheric plume rise and ash dispersal. Modeling results are then

73   compared to available field and satellite data for a first semi-quantitative validation of

74   VOL-CALPUFF.

2.1. Simulation Input Data and Parameters

75   By using the geophysical pre-processors of the system (see *Barsotti et al.* [2007], this

76   issue) an area of 22,500 square km was defined, covering the E part of Sicily and S tip of

77   Calabria. Terrain elevation and land use data were downloaded from the USGS website

78   (http://edc.usgs.gov). Data spatial resolution was about 900 m, even though for visualiza-

79   tion purposes a 90 m DEM of Sicily extracted from the Eurasia SRTM3 archive (available

80   at ftp://e0mss21u.ecs.nasa.gov/srtm/Eurasia) was used. The computational domain was

81   discretized by 150*150 cells with a uniform grid size of 1 km. Meteorological input data

82   needed to run the processor CALMET were provided by the Servizio Idro-Meteorologico of

83   the Emilia Romagna Region (Italy), which runs the non-hydrostatic Limited Area Model

84   Italy (LAMI) (*Doms and Schättler* [1997]; COSMO's web-site [2004]) throughout the

85   Italian territory with a resolution of 0.0625 degrees, equivalent to about 7 km. CAL-

86   MET is then run to compute both the 3D wind field and 2D fields containing the values

87   of the micrometeorological variables used by VOL-CALPUFF to compute atmospheric

88   turbulence parameters (e.g. standard deviations of the horizontal and vertical wind com-

89   ponents). All meteorological fields were computed on 16 terrain-following levels varying

90   between 20 and 8800 m of altitude.

Finally, VOL-CALPUFF needs as input, in addition to the CALMET output, a file containing data characterizing the volcanic source. These inputs include vent altitude and radius, and temperature, pressure, velocity, gas (water vapor) mass fraction and grain size distribution of the eruptive mixture. Table 1 summarizes all performed simulations and the associated vent conditions.

Vent conditions were derived, as much as possible, from the existing published literature and from direct observations described in technical reports. Vent altitude was relatively well constrained. We assumed a value of 2570 m in all simulations performed (*INGV - CT Staff* [2001]; *Calvari and Pinkerton* [2004]; *Scollo et al.* [2007]). Erupted mixture temperature was derived from *Taddeucci et al.* [2004] and fixed at 1300 K, based on residual glass composition, experimentally calibrated geothermometers and assuming no significant cooling effects during magma ascent. Based on the absence of any observed overpressure effects, vent flow pressure was assumed to be atmospheric in all simulations (*Calvari and Pinkerton* [2004]; *Scollo et al.* [2007]). Vent radius, exit flow velocity and water vapor mass fraction are more difficult to estimate through direct measurement, and each parameter was varied within a specific range of values. Vent radius was varied from a few meters up to about 20 m, exit velocity from 20 to 100 m/s and water content from 1.5 to 4.5 *wt%*. Adopted vent radius values (hereafter considered to approximate the plume radius at the vent) are consistent with photo estimates (*Calvari and Pinkerton* [2004]; *Scollo et al.* [2007]). Exit velocities in the 40 - 100 m/s range were estimated by *Scollo et al.* [2007]. The adopted range of water contents (1.5 - 4.5 *wt%*) tries to capture the significant uncertainty associated with this variable, also in light of the possible interaction between the eruptive mixture and external water (the average magma water

114 content estimated by FTIR analyzes of scoriae and lapilli inclusions is about 3.4 $wt\%$

115 (*Metrich et al.* [2004])). The relative effects of these variables, including the influence of

116 the associated mass flow rate, are discussed in the following section. Table 2 reports the

117 granulometric distribution as reconstructed by *Scollo et al.* [2007] on the basis of field

118 work carried out during the eruption and the corresponding μm-size particle distribution

119 assumed at the vent in the performed simulations. The reconstructed distribution is based

120 on the spatial integration of deposit data and does not account for the amount of fine

121 particles dispersed by wind into the far field and inaccessible to field sampling. It should

122 also be pointed out that, although VOL-CALPUFF can potentially treat time-dependent

123 flow conditions at the vent, all simulations were performed under steady-state conditions.

124 In the models, reported temporal variations of plume height and ash dispersal are only

125 caused by changing meteorological conditions.

2.2. Main Results

2.2.1. Plume Rise Phase

127   As already discussed in the companion paper (*Barsotti et al.* [2007], this issue) the rise

128 phase model implemented in VOL-CALPUFF reproduces the contrasting styles charac-

129 terizing an explosive eruption (collapsing, super-buoyant and buoyant) (*Woods* [1988];

130 *Bursik and Woods* [1991]). For the constant vent conditions reported in Table 1, the

131 plume is typically super-buoyant; i.e. the column accelerates upwards after an initial ve-

132 locity decrease. The simulations performed highlight the critical effect of the wind field on

133 column dynamics, not only in terms of eruptive style but also regarding the plume height

134 and dispersal direction. In the presence of a strong wind field the plume axis becomes

135 more tilted toward the ground, whereas a weak wind can generate a higher plume reaching

shorter downwind distances (*Sparks et al.* [1997]; *Bursik* [2001]; *Barsotti et al.* [2007], this issue).

The effect of mass flow rate on column dynamics can be assessed from variations of plume height during the simulated period taking into account the current meteorological conditions. Fig. 2a shows the temporal variation of column height over five days for some of the simulations performed. Due to the significant uncertainty affecting column height, a range of mass flow rate values was chosen for sensitivity tests. The smaller mass flow rates (i.e. *sim_etna1a* and *sim_etna2a*) approximately correspond to the averaged mass flow rates estimated from the deposit volume (see *Scollo et al.* [2007]) when assuming a constant eruption flux over 5 days. As Fig. 2a illustrates, VOL-CALPUFF, for such discharge rates, produces buoyant columns able to rise up to only a few hundreds of meters. By increasing flow rate, ascent behavior changes to super-buoyant and the column reaches greater heights. For comparison, in figure 2a is also reported the approximate range of observed column heights. Some chronicles mention that the column reached a peak height of at least 5500 m above sea level (i.e. about 3000 m above the vent) on 23 July (*Coltelli et al.* [2001]). This observation allows us to use our modeling results in an inverse mode, and to quantify the expected mass flow rate from the column height estimation. It results that an eruption characterized by a mass flow rate in the range $1.5 * 10^4$ (*sim_etna3a*) - $2.5 * 10^4$ (*sim_etna4a*) kg/s can produce an eruptive column able to reach an altitude comparable with that observed. Sensitivity analysis of column height as a function of different velocity/radius values (at a constant mass flow rate and water content) was also carried out (Fig. 2b). Simulation results clearly show how a variation in velocity of 25 - 100 m/s does not change the column height by more than 10%. We therefore fixed the

initial mixture velocity to 25 m/s in most simulations. Lastly, we investigated the effects

of variations in water vapor mass content (Fig. 2c). Variations up to 50% produced

a maximum change in column height of about 15 %, making this a significant variable

(*sim_etna1a-c, sim_etna4a-c, sim_etna6a-c*). In summary, the sensitivity study shows that

the plume mass flow rate is the main volcanological variable controlling column behavior,

with water content also playing a significant role. Variations in velocity/radius values

appear to play a secondary role.

2.2.2. Dispersion of the Ash Cloud and Ground Deposition

Once the plume height has been computed, the VOL-CALPUFF code begins to track

the movements of the puff centers and to calculate the puff diffusion in the defined domain.

The puff feeding rate corresponds to the mass flow rate feeding the rising plume at the vent

minus the amount of mass radially lost by the plume during its ascent. Simulation outputs

consist of the temporal and spatial distribution of particle concentration in air and at the

ground for the nine grain sizes considered (see Table 2). In this section just a few selected

ash dispersal simulation outputs are presented to illustrate the complex and unsteady

cloud dynamics. Some semi-quantitative comparisons with independent observations of

the phenomenon are also made. An initial quantitative description of the large-scale ash

cloud dispersal can be gained by plotting the concentration of the smaller particles in the

eruptive mixture, i.e. the 31 μm particles. These particles can be transported to large dis-

tances even for relatively weak events, such as the 2001 Etna eruption, (*Sparks et al.* [1997])

and, at the same time, they can be detected by satellite thus allowing a semi-quantitative

comparison of modeling results with independent satellite observations (*Rose et al.* [2001];

Bluth and Rose [2004]). Fig. 3 illustrates the evolution of spatial distribution for the total

182 mass of 31 μm particles during the four-day period for simulation *sim_etna4a* starting at

183 00UTC on 20 July (results illustrated every 12 hours). This quantity is obtained by inte-

184 grating the concentration of particles over a column of unitary base up to the maximum

185 extension of the ash plume. It allows dispersal mapping at a given time for a selected par-

186 ticle size. During the first hours of 20 July, fine ash was transported towards Calabria in

187 the NE direction as reported by direct observations. In the following hours the ash cloud

188 started moving towards the E and then S (clockwise rotation of ca. 90 degrees). During

189 22 July the ash cloud passed several times over Catania showing a series of fluctuations

190 in the S-SE directions. Finally, on 23-24 July the cloud remained mainly directed SE. An

191 initial quantitative comparison between modeling results and observations can be made

192 by using satellite images. A number of similar comparisons were carried out at different

193 times during the four days of dispersal for different mass flow rates and the agreement

194 between remote sensing observations and predictions for the finer ash distribution was

195 always a close one. Fig. 4 presents the comparison between the dispersal patterns of the

196 different granulometric classes of *sim_etna4a* (characterized by a mass flow rate of $2.5*10^4$

197 kg/s), as computed by VOL-CALPUFF, and NOAA/AVHRR satellite image (available

198 at the web site http://www.nerc-pml.ac.uk/rsdas/projects/etna/pic_gallery.html). The

199 comparison refers to 1114UTC on 20 July. For comparison purposes, 3 μm particles were

200 also considered in the simulation to evaluate the behavior of micron-size particles. Figure

201 4 illustrates the spatial distribution of the total mass of each particle size obtained by

202 vertically integrating the concentration of each class over the entire plume height. It can

203 be seen that the 3 and 31 μm particles closely follow the dispersal pattern apparent in

204 the satellite image (E-NE), matching the main dispersal axis and the lateral extension of

₂₀₅ the detected plume, whereas all the other particles are transported in different directions

₂₀₆ not detected by satellite. In particular, particles of 62 and 125 μm seem to move firstly

₂₀₇ towards E and then slightly deviate towards the S-SE direction. Similarly, the larger re-

₂₀₈ ported particles (250 μm and 2 mm) show a totally independent movement, characterized,

₂₀₉ from the beginning, by a northward displacement.

₂₁₀   In order to better understand the reason for such a complex dispersal pattern some

₂₁₁ features of the wind field around the volcano were investigated. Fig. 5 shows the wind

₂₁₂ field streamlines at the levels of 400 and 2200 m a.g.l computed by the meteorological

₂₁₃ pre-processor CALMET for the acquisition time of the satellite image shown in Fig. 4.

₂₁₄ As expected, at levels closer to the ground the wind is strongly affected by the volcano's

₂₁₅ topography thus generating a more irregular field, whereas at higher altitudes the wind

₂₁₆ shows a quasi-geostrophic trend.

₂₁₇   A more complete picture of the wind field spatial and temporal variability, as produced

₂₁₈ by the CALMET code, can be gained by analysing the wind direction and speed at

₂₁₉ different altitudes. Fig. 6 describes variations of wind direction and speed over four days

₂₂₀ (21-24 July) above the vent area, 15 km E and 15 km S from the vent, at two different

₂₂₁ altitudes above the ground (400 and 2200 m). A key result is the strongly irregular

₂₂₂ patterns of the flow field close to the ground (400 m) (see Figs. 6a and 6c), above the

₂₂₃ vent and 15 km S and E. This irregularity is particularly pronounced for wind direction.

₂₂₄ At the vent and at a location 15 km E of it, wind direction varies by 90-130 degrees over

₂₂₅ the four days (blowing towards W above the vent and towards E some 15 km E from it).

₂₂₆ These variations become even more dramatic 15 km S of the vent where three inversions of

₂₂₇ 180 degrees, between the evening of the 23 and the evening of the 24 July, are predicted.

228   In contrast, at 2200 m a.g.l the wind is blowing from NW to SE on almost any day of

229   the investigated period with a speed on the first day about five times greater than that

230   at lower levels. Wind speed at high altitude remains twice near-ground wind speed on all

231   other days.

232   VOL-CALPUFF can be used to estimate ground deposition as a function of assumed

233   particle size distribution and mass flow rate. Fig. 7 illustrates particle deposition for six

234   of the nine granulometric sizes employed in the *sim_etna4a* simulation. Deposition refers

235   to total ash accumulation over four days, between 21 and 24 July. We considered this

236   shorter period because of the availability of deposit measurements (*Scollo et al.* [2007])

237   which enable the comparison of model predictions with deposit data (see hereafter). It

238   is evident from the figure how the various particles disperse and deposit following very

239   different dynamics. On figure 7, the smaller particles (e.g. 31 μm) are mostly transported

240   in the direction of the prevailing high-altitude winds and remain confined in the SE

241   quadrant. Intense wind quickly advects these low settling velocity particles out of the

242   domain, so that the deposit iso-contours show values up to several orders of magnitude

243   smaller than those of the other particles sizes. In contrast, for increasingly large particles

244   the location of maximum deposition moves towards the vent, as expected. 500 μm and

245   1 mm particles are much less dispersed than finer particles and their deposit is more

246   uniform in the azimuthal direction. Similar patterns were obtained for the 2, 4 and 8 mm

247   particles.

248

249   By summing the partial deposits produced by the nine different particle sizes it is

250   possible to compute the total particle accumulation. Fig. 8a and 8c show the mass isolines

²⁵¹ of ash deposited after four days of activity for the two mass flow rates (i.e. 1.5 and 2.5 $*10^4$

²⁵² kg/s) suggested as end-member values for the event investigated (*sim_etna3a, sim_etna4a*).

²⁵³ Fig. 8b and 8d show a comparison of the two computed deposition patterns with the

²⁵⁴ deposit measurements, in kg/m^2, as reported by *Scollo et al.* [2007]. The total deposit

²⁵⁵ isolines show a quite irregular and non-symmetric pattern in both cases. Both results

²⁵⁶ present a deposit characterized by a preferred E-SE direction, due to higher columns that

²⁵⁷ inject material at atmospheric levels characterized by intense wind, which, as we have

²⁵⁸ already seen (Fig. 6b), blew most of the time towards this quadrant. The predicted

²⁵⁹ deposit distributions show that maximum deposition is at a few kilometers from the vent

²⁶⁰ in the S-SE direction, as in the measured deposit (*Scollo et al.* [2007]). The lower end-

²⁶¹ member mass flow rate (Fig. 8a and Fig. 8b - *sim_etna3a*) produces a deposit which

²⁶² fits the sampled data with a correlation coefficient of 0.77 and with more than 97% of

²⁶³ simulated data ranging from 1/5 to 5 times the observed values. For the larger end-

²⁶⁴ member mass flow rate (Fig. 8c and Fig. 8d - *sim_etna4a*) the numerical prediction

²⁶⁵ largely overestimates the amount of ash deposited. A comparison between computed and

²⁶⁶ measured values quantifies this discrepancy to be up to about a factor of 5.

3. Discussion

²⁶⁷ The above results show that VOL-CALPUFF is helpful to investigate ash dispersal

²⁶⁸ processes. The new model captures the strong influence of meteorological conditions on

²⁶⁹ plume rise dynamics, shows the necessity to use codes able to determine column height

²⁷⁰ using a plume rise model and the importance of using an accurate meteorological data

²⁷¹ set. A useful result that can be inferred *a posteriori* from modeling of column height in

²⁷² the presence of realistic meteorological conditions is the estimation of the mass flow rate

feeding the plume. For the 2001 Etna event, the results reported in Fig. 2 illustrate that only mass flow rates between $1.5 * 10^4$ kg/s (*sim_etna3a*) and $2.5 * 10^4$ kg/s (*sim_etna4a*) are likely able to produce a maximum column height of about 3000 m above the vent on 23 July. Based on the analysis reported in the companion paper (see Fig. 4 of *Barsotti et al.* [2007], this issue) on the effect of the entrainment coefficients and the values here assumed, these values should be considered as minimum values in order to reproduce the observed column height. In contrast, using an *averaged* mass flow rate, obtained by dividing the total amount of mass erupted ($1.02 * 10^9$ and $2.31 * 10^9$ kg from *Scollo et al.* [2007]) by event duration (*sim_etna1a* and *sim_etna2a*), it would not be possible to match the observed column height. Only in a still environment, the plume could reach altitudes comparable with observed ones if fed with averaged mass flow rates (as assumed in *Costa et al.* [2006]). For the long-lasting weak plume considered here, the assumption of an average mass flow rate is inadequate to simulate the whole dispersal process, since it strongly underestimates column height. However the range of mass flow rate estimated above from the column height (*sim_etna3a* and *sim_etna4a*) is likely representative of the *peak* mass flow rate. This could significantly overestimate the erupted volume and ash ground deposition. If we consider the column height and deposit estimates, we see that each of the two end-member values matches only one of the two observed variables. Plume feeding with a steady mass flow rate of $1.5 * 10^4$ kg/s allows a match with the amount of material deposited (see Fig. 8b), but the predicted column height only approximately matches the minimum observed values (see Fig. 2a). By feeding the plume with the higher mass flow rate (i.e. $2.5 * 10^4$ kg/s) it is possible to match the observed plume height but not deposit estimates (Fig. 8d). A reasonable explanation for this discrepancy is that events lasting

²⁹⁶ several days, such as the 2001 Etna eruption, are characterized by unsteady, intermittent

²⁹⁷ plume feeding (*INGV - CT Staff* [2001]; *Taddeucci et al.* [2004]; *Scollo et al.* [2007], P. Al-

²⁹⁸ lard written communication (2007)). Plume-feeding is therefore quite difficult to quantify

²⁹⁹ and sometimes also hard to detect (for instance during nocturnal periods or bad weather

³⁰⁰ conditions).

³⁰¹ We believe that a better match between modeling results and observations cannot be

³⁰² achieved under the assumption of steady-state plume feeding over the investigated four-

³⁰³ day period. The few available measurements are affected by significant uncertainty and

³⁰⁴ do not allow more accurate comparison or the definition of time-dependent plume feeding

³⁰⁵ over the simulated period. In order to support this interpretation we performed addi-

³⁰⁶ tional simulations adopting two different mass flow rates for the plume and puffs. We ran

³⁰⁷ VOL-CALPUFF assuming a mass flow rate of $2.5*10^4$ and $1.0*10^4$ kg/s for the plume

³⁰⁸ and puff release, respectively. In this way we were able to match the observed column

³⁰⁹ height and produce a deposit distribution (not shown) that fits the measured values with

³¹⁰ a correlation coefficient (R=0.82) higher than that for the simulations reported in Fig. 8.

³¹¹ Another variable that could significantly reduce the above discussed discrepancy is the

³¹² gas mass fraction of the eruptive mixture at the vent. Water contents greater than those

³¹³ assumed here could favor higher columns for a given mass flow rate (Fig. 2c).

³¹⁴ VOL-CALPUFF allows analysis of new and non-intuitive effects of ash dispersal in an

³¹⁵ orographically complex area under the action of 3D meteorological conditions. These

³¹⁶ effects are apparent in the dispersal behavior of contrasting particles sizes. The major

³¹⁷ mass *splitting* effect we observe in Fig. 4 and Fig. 7 between particles of different sizes

³¹⁸ is the result of two main factors: (a) the dependence of settling velocities on particle

dimension and density and (b) the great variability and complexity of wind field patterns in the vertical and horizontal directions. These factors make larger particles cross the atmosphere in a temporal interval up to two orders of magnitude faster than the smaller particles (minutes vs. hours), travelling faster towards the ground where wind fields are more irregular. Particles up to a few tens of microns remain much longer at high atmospheric levels, where more uniform winds take them far from the vent. These results are in agreement with the very first attempt to investigate the control of wind-shear and grain size distribution on ash dispersal by *Woods et al.* [1995]. In terms of validation of the predicted particle dispersal behavior, an initial comparison of simulation outputs with satellite images was carried out. Results suggest that VOL-CALPUFF is able to correctly predict the dispersal of the smaller particles moving at high altitude above the ground. The path observed in satellite images was closely followed by particles up to about 30 μm in our simulations. In contrast, the AVHRR satellite images taken by the NOAA satellite do not show the more irregular behavior that the simulations produce for particles larger than about 30 μm. This result is consistent with the present limitations of satellite remote sensing techniques in detecting suspended material with a radius greater than a few tens of microns (*Wen and Rose* [1994]; *Yu and Rose* [2002]; *Bluth and Rose* [2004]). Given the importance, in terms of mass dispersed in the atmosphere, of particles with size in the range 62 μm-1 mm (see Table 2), an important contribution to the detection of these coarse particles should come from the use of other remote sensing techniques such as weather radar observation (*Lacasse et al.* [2004]; *Marzano and Vulpiani* [2006]). Unfortunately, such data are not available for the 2001 Etna event and cannot be used to validate the numerical predictions. This type of investigation appears particularly im-

portant for particle sizes (e.g. 125 μm) that can reach concentrations of a few g/m^3 far away from the area indicated by the satellite images. Such concentrations are well above those used by other ash forecasting codes as a threshold for ash cloud visibility (*Simpson et al.* [2002]). Qualitative support for the modeling results here presented comes from the observation that ash fallout of coarse particles was actually recorded several times, during the 2001 event, well away from the main plume dispersal direction (Andronico D., personal communication, 2005).

From the above discussion the fundamental role played by meteorology in the determination of both plume rise and ash dispersal is evident. A better understanding of the minimum resolution of meteorological data required to capture, with sufficient accuracy, most of the results illustrated here, is necessary for future progress. The present modeling results could also contribute towards a more quantitative interpretation of remote sensing and field data.

4. Conclusions

The first application of VOL-CALPUFF, to the 2001 explosive event of Mt. Etna, highlights new key features of the dynamics of weak volcanic plumes in the presence of a complex wind field. Some of the most important aspects are: (a) the major effect of the wind field in the determination of the column height and bending, as well as of plume ascent style, (b) the great difference in the dispersal patterns followed by ashes of different sizes producing a very complex and non-intuitive dispersal, (c) the complex distribution of ash on the ground showing preferential directions of dispersal and, for events characterized by long duration and variable winds, a quite irregular deposit pattern, (d) the impossibility to reproduce both column height and deposit features by adopting

a vent steady-state mass flow rate due to temporal variations in plume feeding during the four-day period investigated. Furthermore, this initial application of VOL-CALPUFF to weak plumes poses new questions about the use of low-resolution meteorological data for the accurate prediction of the complex ash dispersal and fallout dynamics. Finally, it highlights, once more, the importance of comparing modeling results to accurate field data and observations in order to reach a consistent understanding of the dispersal dynamics and also prompts new developments in modeling and observational techniques.

References

Barsotti S., A. Neri and J. S. Scire (2007), The VOL-CALPUFF Model for Atmospheric Ash Dispersal: I. Approach and Physical Formulation, submitted to *J. Geophys. Res.*.

Bluth, G. J. S. and W. I. Rose (2004), Removal processes of volcanic ash particles from the atmosphere, Proceedings of 2nd International Conference on Volcanic Ash and Aviation

385   Safety, VAAS, pp. 51–54, OFCM, Alexandria, Virginia, USA, June 21-24.

386   Bursik, M. I. and A. W. Woods (1991) Buoyant, superbuoyant and collapsing eruption

387   columns, *J. Volcanol. Geotherm. Res.*, *45*, 347–350.

388   Bursik, M. I. (2001), Effect of wind on the rise height of volcanic plumes, *Geophys. Res.*

389   *Lett.*, *28*(18), 3621–3624.

390   Calvari, S. and H. Pinkerton (2004), Birth, growth and morphologic evolution of the

391   'Laghetto' cinder cone during the 2001 Etna eruption, *J. Volcanol. Geotherm. Res.*,

392   *132*, 225–239.

393   Coltelli, M., P. Del Carlo and G. Macedonio (2001), The plume of the 2001 eruption of

394   Etna: Observation, modeling and impact on Catania airport operations, Proceedings

395   of GNV General Assembly, p. 222, GNV, Rome, Italy, October 9-11.

396   Costa, A., G. Macedonio and A. Folch (2006), A three-dimensional Eulerian model for

397   transport and deposition of volcanic ashes, *Earth and Science Planetary Letters*,*241*,

398   634–647.

399   Consortium for Small-scale Modeling (COSMO)'s web-site: http://cosmo-model.cscs.ch/

400   Doms, G. and U. Schättler (1997), The Nonhydrostatic Limited-Area Model LM (Lokal-

401   Model) of DWD, Part I: Scientific Documentation, Deutscher Wetterdienst (DWD),

402   Offenbach, March 1997.

403   Environmental Protection Agency U.S. (1998), Interagency Workgroup on air quality

404   modeling (IWAQM) Phase 2: Summary report and recommendations for modeling long

405   range transport impacts, EPA-454/R-98-019, Office of Air Quality Planning and Stan-

406   dards, U. S. EPA, Research Triangle Park, NC 27711.

407   GVP/USGS Volcano Archive: www.volcano.si.edu/gvp/reports/usgs/archive.cfm

INGV - CT Staff (2001), Rapporti tecnici 20 - 24 July 2001. www.ct.ingv.it.

Lacasse, C., S. Karlsdottir, G. Larsen, H. Soosalu, W. I. Rose and G. G. J. Ernst (2004), Weather radar observations of the Hekla 2000 eruption cloud, Iceland, *Bull. Volcanol*, *66*, 457-473.

Marzano, F. S., G. Vulpiani and W. I. Rose (2006), Microphysical characterization of microwave radar reflectivity due to volcanic clouds, *IEEE TGRS*, doi: 10.1109/TGRS.2005.861010.

Metrich N., P. Allard, N. Spilliaert, D. Andronico and M. Burton (2004), 2001 Flank eruption of the alkali- and volatile-rich primitive basalt responsible for Mount Etna's evolution in the last three decades, *Earth and Science Planetary Letters*, *228*, 1–17.

Nguyen, K. C., J. A. Noonan, I. E. Galbally and W. L. Physick (1997), Predictions of plume dispersion in complex terrain: Eulerian versus Lagrangian models, *Atmos. Environ.*, *31*(7), 947–958.

Rose, W. I., G. J. Bluth, D. J. Schneider, G. G. J. Ernst, C. M. Riley, L. J. Henderson, and R. G. McGimsey (2001), Observations of 1992 Crater Peak/Spurr volcanic clouds in their first few days of atmospheric residence, *J. Geol.*, *109*, 677–694.

Scire, J. S., D. G. Strimaitis and R. J. Yamartino (2000), CALPUFF User's guide. Earth Tech, Inc., Concord, MA, available at web-site: http://www.src.com/calpuff/download/download.htm

Scollo, S., P. Del Carlo and M. Coltelli (2007), Tephra fallout of 2001 Etna flank eruption: Analysis of the deposit and plume dispersion, *J. Volcanol. Geotherm. Res.*, *160*, 147–164.

Simpson, J. J., G. L. Hufford, R. Servranckx, J. S. Berg and C. Bauer (2002), The February 2001 eruption of Mt.Cleveland, Alaska: Case study of an aviation hazard, *American Meteor. Soc.*, *17*, 691–704.

Sparks, R. S. J., M. I. Bursik, S. N. Carey, J. S. Gilbert, L. S. Glaze, H. Sigurdsson and A. W. Woods (1997), *Volcanic plumes*, .Wiley, New York .

Taddeucci, J., M. Pompilio and P. Scarlato (2002), Monitoring the explosive activity of the July-August 2001 eruption of Mt.Etna (Italy) by ash characterization, *Geophys. Res. Lett.*, *29*(8), 1230, doi:10.1029/2001GL014372.

Taddeucci, J., M. Pompilio and P. Scarlato (2004), Conduit processes during the July-August 2001 explosive activity of Mt.Etna (Italy): Inferences from glass chemistry and crystal size distribution of ash particles, *J. Volcanol. Geotherm. Res.*, *137*, 33–54.

Wen, S. and W. I. Rose (1994), Retrieval of sizes and total masses of particles in volcanic clouds using AVHRR bands 4 and 5, *J. Geophys. Res.*, *99*, 5421–5431.

Woods, A. W. (1988), The fluid dynamics and thermodynamics of eruption columns, *Bull. Volcanol.*, *50*, 169–193.

Woods, A. W., R. E. Holasek and S. Self (1995), Wind-driven dispersal of volcanic ash plumes and its control on the thermal structure of the plume-top, *Bull. Volcanol.*, *57*, 283–292.

Yu, T. and W. I. Rose (2002), Atmospheric correction for satellite-based volcanic ash mapping and retrievals using split window IR data from GOES and AVHRR, *J. Geophys. Res.*, *107*, 4311–4327.
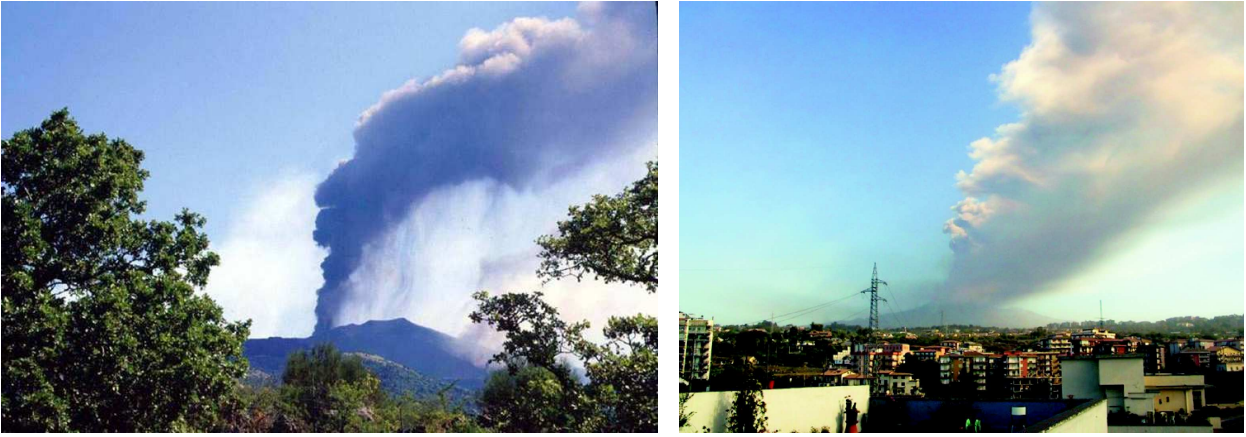
Figure 1.   Photographs of the volcanic plume and ash fallout over Catania and nearby villages, during the recent eruptive events at Mt.Etna. Photos by P. Papale (INGV Pisa) and from www.larepubblica.it, respectively.

Table 1.   List of performed simulations. The table contains the input data values
assumed at the vent. V is velocity, R vent radius, H_2O the weight percent of water vapor
and mfr the resulting mass flow rate. Vent radius was derived from the other three
variables by using the mass conservation equation. Vent altitude, vent flow temperature
and exit mixture pressure were kept constant in all simulations and are equal to 2570 m,
1300 K and atmospheric value, respectively. As explained in *Barsotti et al.* [2007] (this
issue) all the simulations were performed using entrainment coefficients values (α and γ)
equal to 0.09 and 0.6, respectively.

Name	V (m/s)	R (m)	H_2O (wt%)	mfr (kg/s)
sim_etna1a	20	2.7	3	$2.0 * 10^3$
sim_etna1b	30	2.7	4.5	$2.0 * 10^3$
sim_etna1c	25	1.7	1.5	$2.0 * 10^3$
sim_etna2a	20	4.8	3	$6.6 * 10^3$
sim_etna3a	25	6.7	3	$1.5 * 10^4$
sim_etna4a	25	8.7	3	$2.5 * 10^4$
sim_etna4b	30	9.7	4.5	$2.5 * 10^4$
sim_etna4c	25	6.2	1.5	$2.5 * 10^4$
sim_etna4d	50	6.2	3	$2.5 * 10^4$
sim_etna4e	75	5	3	$2.5 * 10^4$
sim_etna4f	100	4.3	3	$2.5 * 10^4$
sim_etna5a	25	11	3	$4.0 * 10^4$
sim_etna6a	25	15.1	3	$7.5 * 10^4$
sim_etna6b	30	16.7	4.5	$7.5 * 10^4$

Name	V (m/s)	R (m)	H_2O (wt%)	mfr (kg/s)
sim_etna6c	25	10.6	1.5	$7.5 * 10^4$
sim_etna6d	50	10.6	3	$7.5 * 10^4$
sim_etna6e	75	8.7	3	$7.5 * 10^4$
sim_etna6f	100	7.5	3	$7.5 * 10^4$
sim_etna7a	25	19.86	3	$1.3 * 10^5$

Table 2.   The particle size distribution of the eruptive mixture assumed at the vent in the simulations performed as coming from the reconstructed total granulometric distribution (*Scollo et al.* [2007]).

Φ	Diameter (μm)	wt%
-3	8000	0.11
-2	4000	0.69
-1	2000	2.47
0	1000	7.53
1	500	20.36
2	250	40.2
3	125	24.06
4	62	3.89
5	31	0.69
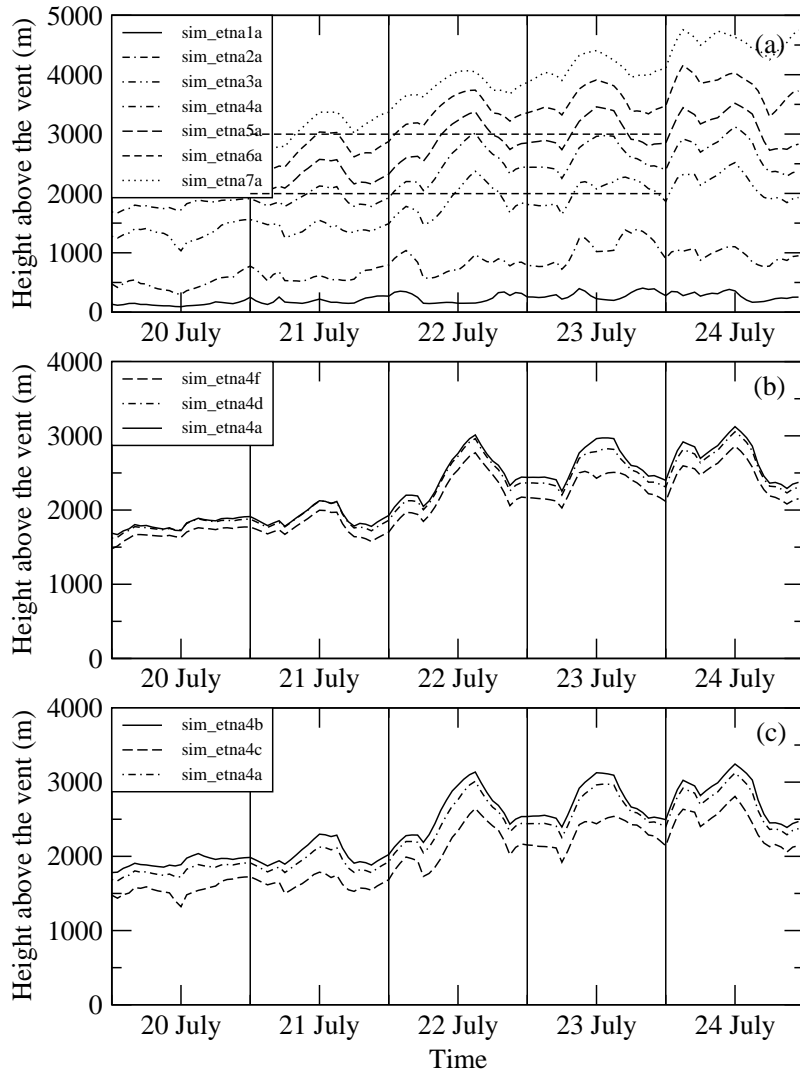
Figure 2. Temporal variations of column height as computed by VOL-CALPUFF for some of the simulations reported in Table 1. (a) Comparison between column heights computed for plumes with different mass flow rates. The vent mass flow rate is kept constant in time during each simulation. The superimposed horizontal lines delimit the observed range for the 21-23 July period (*Scollo et al.* [2007]); (b) Comparison between column heights computed for plumes with different mixture velocities (at constant mass flow rate and water content); (c) Comparison between column heights computed for plumes with different water vapor mass fractions.
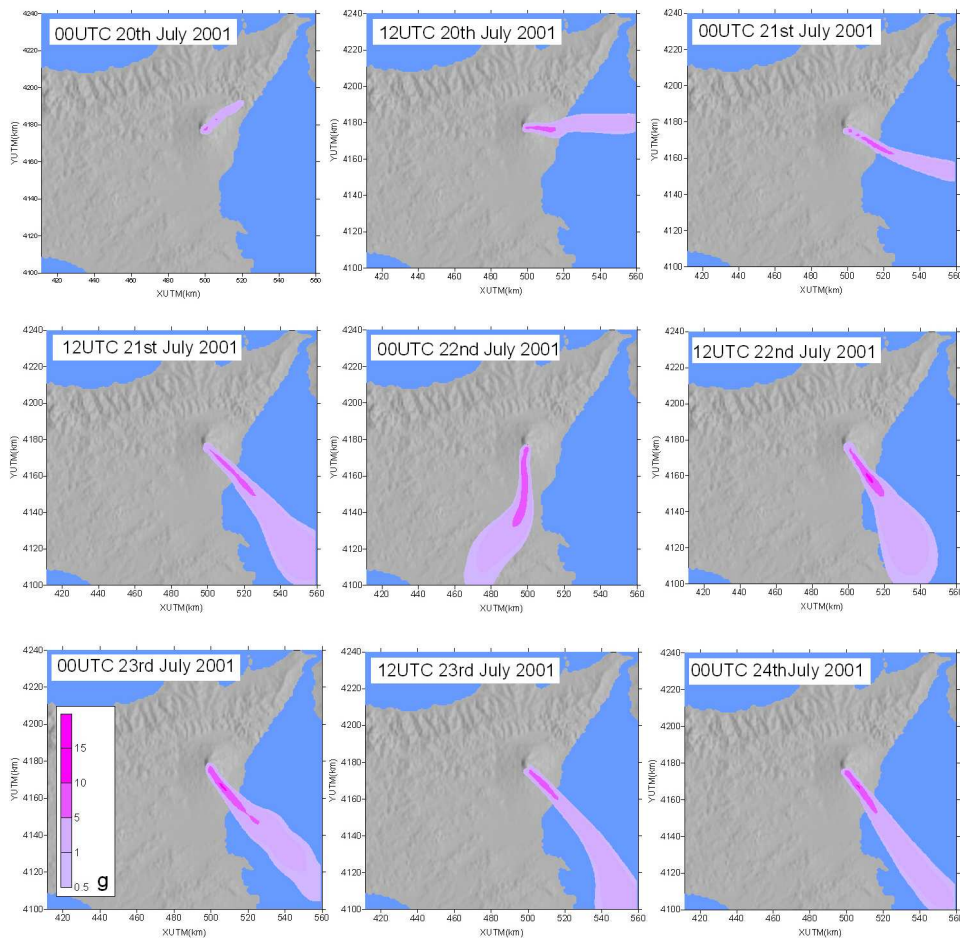
Figure 3.   Cumulative mass of 31 μm particles, obtained by integration of its concentration over all vertical levels in the atmosphere. From the upper left-hand corner the concentration is mapped each 12 hours starting at 00UTC on 20 July. Isocontour values are reported on the bottom left-hand corner and refer to the total mass in grams. Results from simulation *sim_etna4a*.
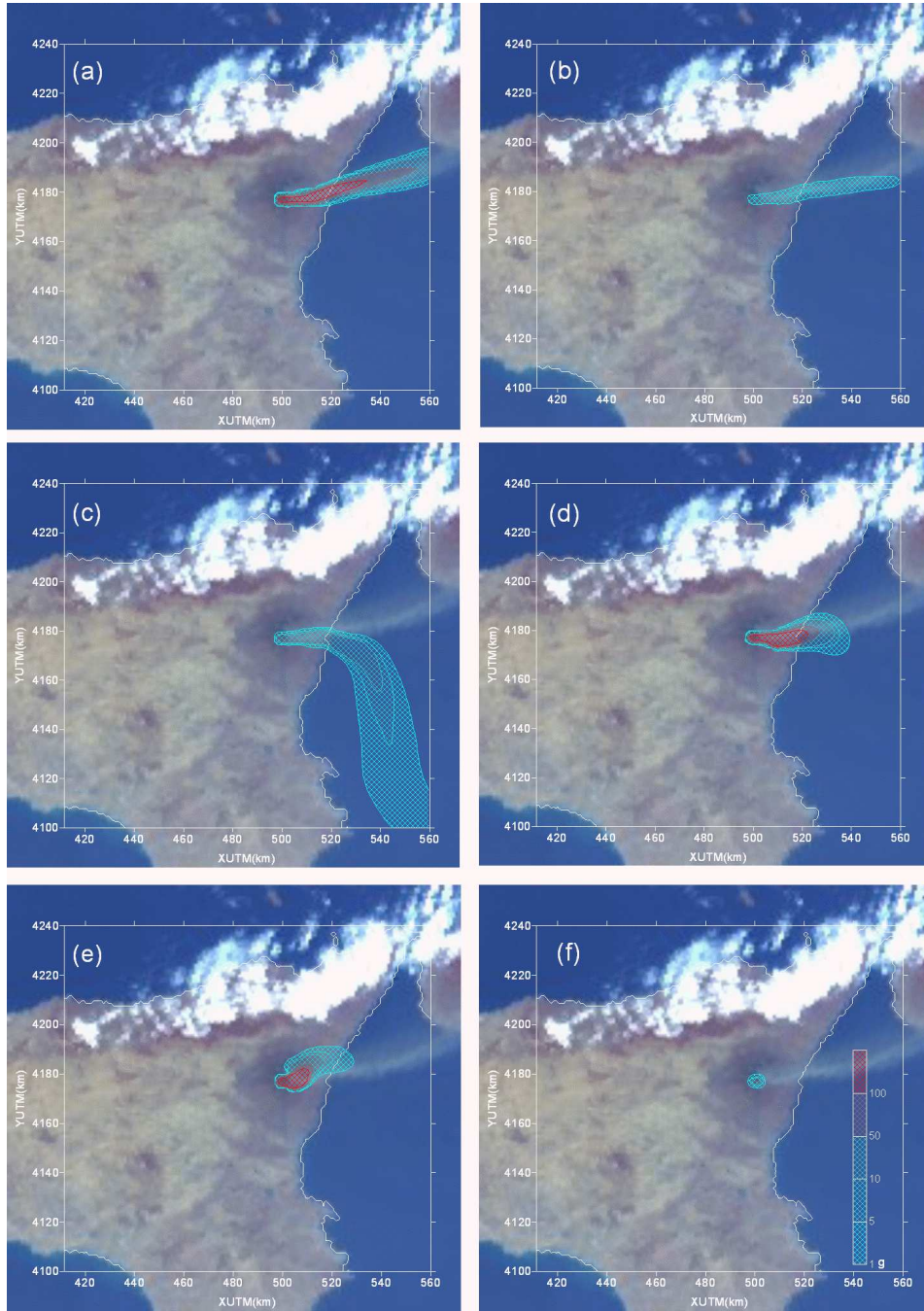
Figure 4.   SeaStar satellite image at 1114UTC on 20 July compared with *sim_etna4a*
results. The figures show the amount of ash integrated in the vertical extension of the
domain for six different classes (3 (a), 31 (b), 62 (c), 125 (d), 250 (e) μm and 2 mm (f)).
In all images the minimum reported isocontour is equal to 1 g. The comparison shows how
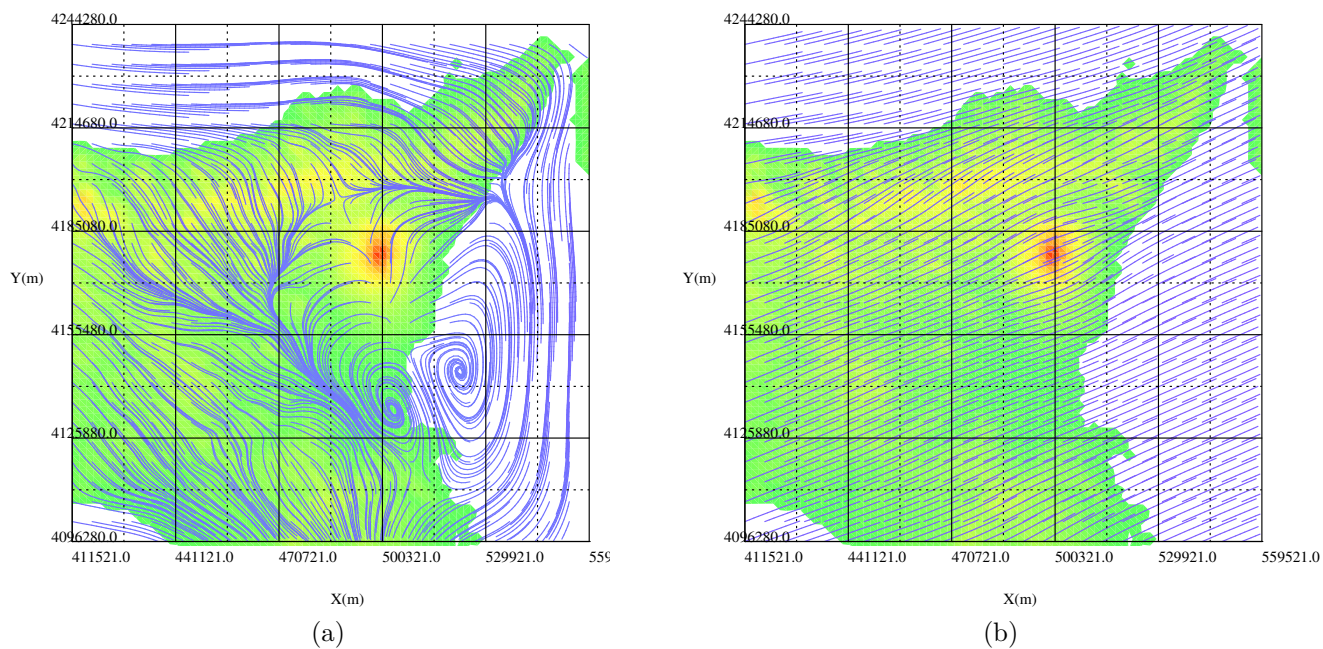the detection of the plume by the satellite image is limited to the detection of particles of
a few-μm (*Bluth and Rose* [2004]).

Figure 5. Wind field streamlines, as produced by CALMET model, at 400 m (a) and 2200 m (b) above ground level at 1100UTC on 20 July.
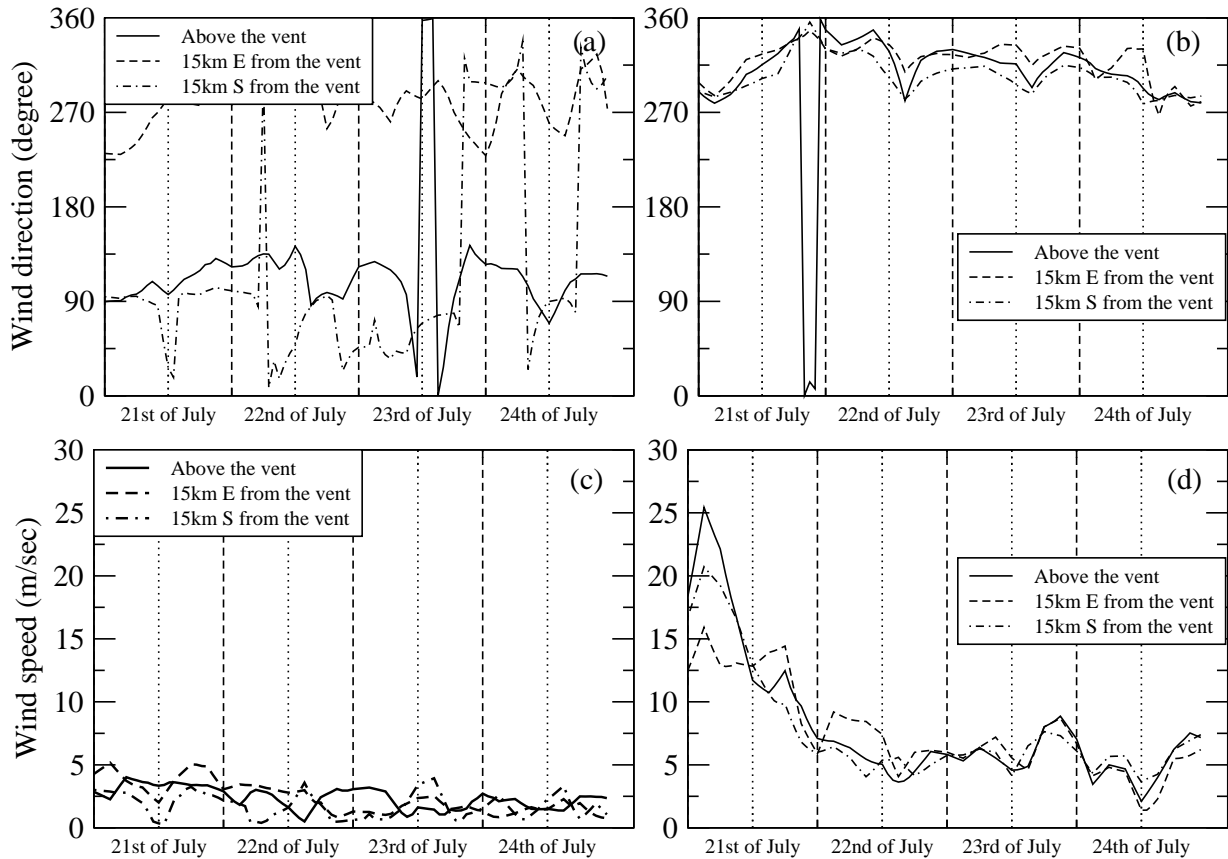
Figure 6. Temporal variations of wind direction (a and b) and wind speed (c and d) at different spatial locations. The wind information, produced by the CALMET model, is reported hourly for three different locations: above the vent, 15 km from the vent toward E or S. Wind information related to a terrain-following vertical level at 400 m agl (a and c) are compared with the same informations obtained for a 2200 m terrain-following level (b and d). The figures illustrate the effects on low atmosphere wind direction caused by complex orography (the effect of eruption dynamics on local atmospheric conditions is not considered by the model). At a higher level the wind field is more regular and faster than closer to the ground.
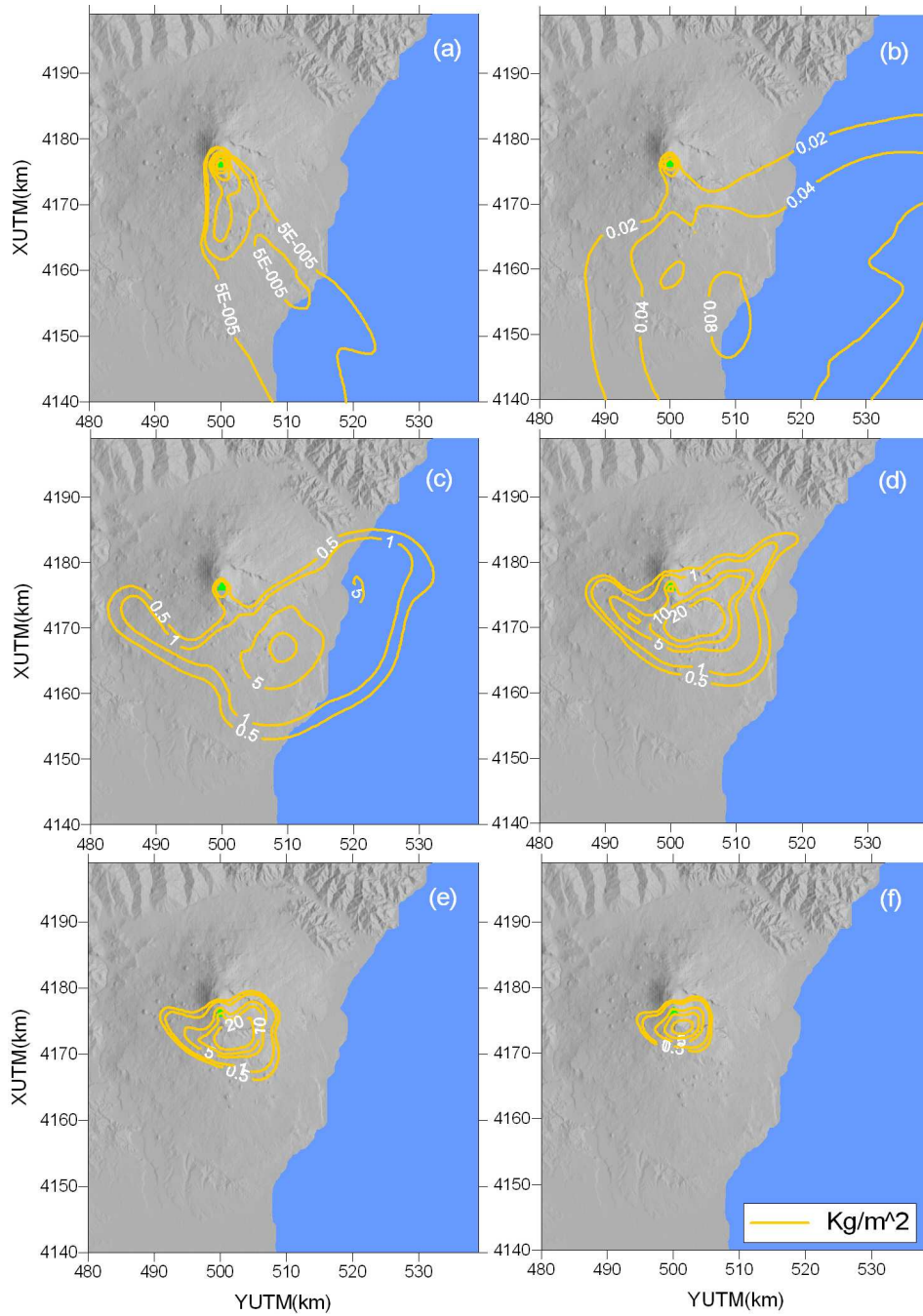
Figure 7. Ground deposit as a function of particle diameter for an emission rate of $2.5 * 10^4$ kg/s (*sim_etna4a*) over four days (21-24 July). Six classes with diameter of (a) 31 μm, (b) 62 μm, (c) 125 μm, (d) 250 μm, (e) 500 μm and (f) 1 mm are reported. Particles with larger diameters show a behavior similar to the 1 mm particles.
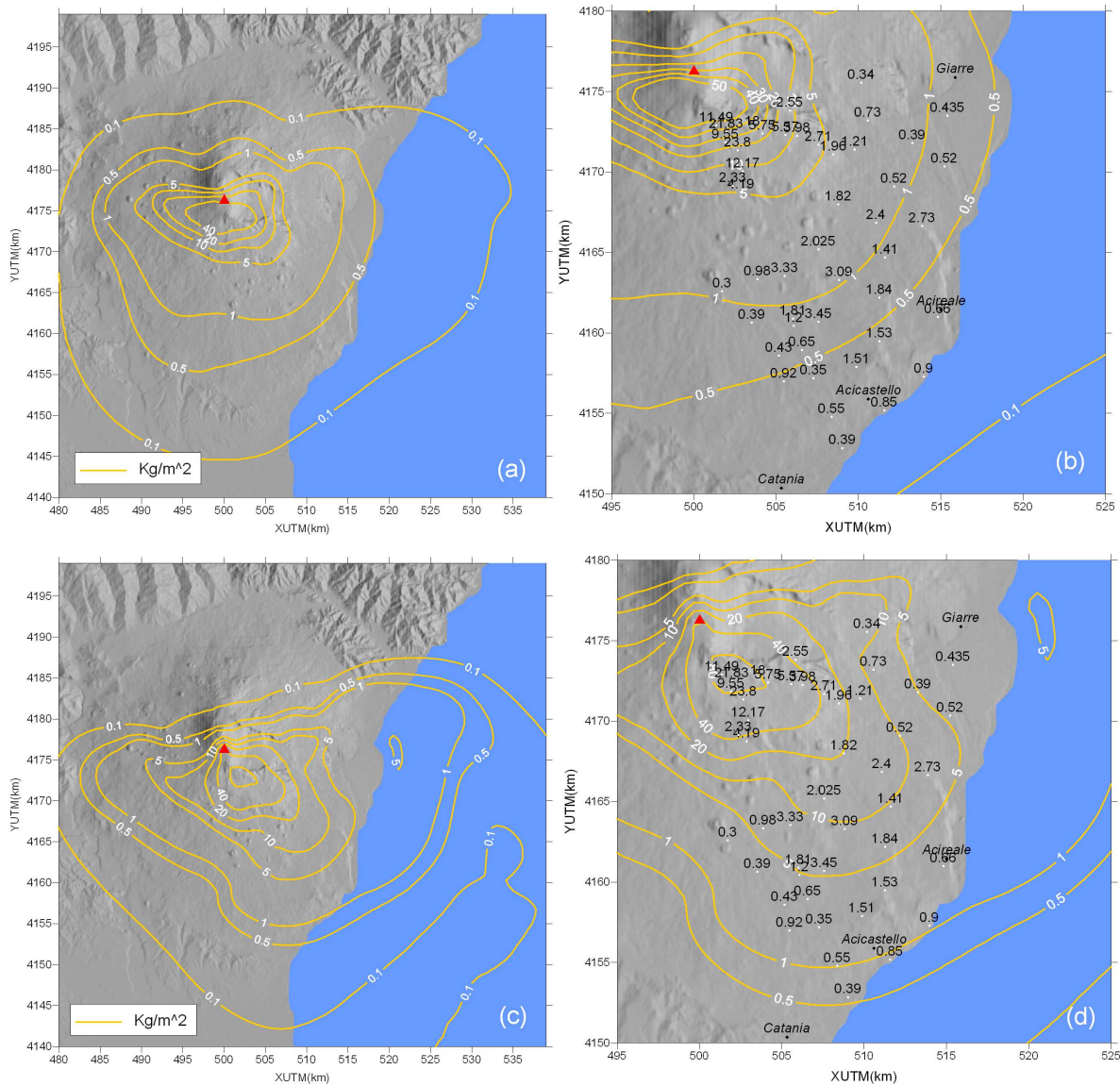
Figure 8. Total accumulation on the ground of all particle sizes after four days (21-24 July) of steady ash emission. A comparison between two different mass flow rates, i.e. $1.5 * 10^4$kg/s (*sim_etna3a*) (a, b) and $2.5 * 10^4$ kg/s (*sim_etna4a*) (c, d), is shown. Both deposit patterns are characterized by an irregular shape with a peak at some kms from the vent ((a) and (c)). A zoomed comparison with measured field data (from *Scollo et al.* [2007]) highlights a good agreement for the case *sim_etna3a* (correlation coefficient R = 0.77) (b), and an overestimation up to about a factor of 5 for the case *sim_etna4a* (d).